This article has been accepted for inclusion in a future issue of this journal. Content is final as presented, with the exception of pagination.

Current Balancing Technique for the High-Current Windings of Medium-Frequency Transformers

Reza Mirzadarani, *Student Member, IEEE*, Zhengzhao Li, *Student Member, IEEE*, Zian Qin, *Senior Member, IEEE*, Peter Vaessen, *Member, IEEE*, Pavol Bauer, *Senior Member, IEEE*, and Mohamad Ghaffarian Niasar, *Member, IEEE*

***Abstract*—This study presents a current balancing technique for high-current windings in medium-frequency transformers (MFTs), particularly relevant to solid-state transformer (SST) applications. Handling high currents on the low-voltage high-current winding of MFTs is challenging due to skin and proximity effects. Conventional techniques, such as continuously transposed conductors (CTCs) and parallel winding paths, are applicable but have limitations in medium-and high-frequency applications such as SSTs due to skin and proximity effects. To address these issues, a modular and tunable compensation method is proposed, based on adding small, series-connected inductive elements (compensation toroids) to each parallel winding path. Experimental results from a prototype validate the proposed compensation technique, highlighting its effectiveness in mitigating unbalanced current distribution. Finite element analysis (FEA) and experimental validation across a wide frequency range (1–10 kHz) confirm the effectiveness of the method. The results demonstrate a significant reduction in current imbalance with minimal added losses or system impact.**

***Index Terms*—Current sharing, loss mitigation, solid-state transformer (SST).**

I. Introduction

SOLID-STATE transformers (SSTs) have gained significant attention recently due to their potential for high-power applications, such as green hydrogen production [2], [3], [4], [5]. These advanced converters offer several advantages over traditional transformers, including enhanced efficiency, improved power quality, and greater flexibility in grid integration [6]. As SSTs are increasingly employed in high-power applications, they are commonly connected to medium-voltage grids and tasked with supplying relatively low-voltage loads such as green-hydrogen electrolyzers [8], [9]. This operational scenario necessitates handling high currents on the secondary side. Meanwhile, SSTs typically contain medium frequency transformers. Handling high currents at such a frequency requires innovative solutions.

To manage high current in transformer windings, a number of current-handling techniques have been employed in both low- and medium-frequency applications. These include the use of continuously transposed conductors (CTCs) and parallel winding paths, which help distribute current and reduce skin and proximity effects. However, these methods show limitations at medium frequencies, where proximity effects become dominant and winding geometry plays a larger role [10], [11], [12]. CTCs can mitigate the skin effect significantly; nevertheless, the impact of the core and the proximity effect become dominant when the applied frequency is higher. Implementing a number of parallel paths addresses practical issues when big conductors are needed to handle the high current. However, the proximity effect is again problematic.

In low-frequency, high-current transformers, such as arc furnace transformers, additional techniques such as geometric modifications (e.g., varying disk diameters, winding height, or spacing) are employed to improve current sharing [7], [10], [13]. While effective at 50/60 Hz, these geometrical methods become impractical at higher frequencies due to the need for significant variations and increased construction complexity. In addition, SSTs face additional complexities since the operation under high-or medium-frequency excitation leads to enhanced proximity and skin effects, exacerbating high current issues [14]. While litz wires are a viable solution for low-voltage power electronics applications to mitigate these effects, they are impractical for medium-voltage, medium-frequency SSTs [15].

The literature on SSTs and high-current handling techniques is extensive. Prior research has explored various aspects of SST design, including their efficiency, thermal management, and electromagnetic performance [8], [16], [17], [18], [19], [20], [21], [22], [23]. Studies on arc furnace transformers have

Received 16 June 2025; revised 9 September 2025; accepted 1 October 2025. This work was supported by the RVO MOOI (Missiegedreven Onderzoek Ontwikkeling en Innovation) under Grant MOOI 52103. *(Corresponding author: Mohamad Ghaffarian Niasar.)*

The authors are with the Department of Electrical Sustainable Energy, TU Delft, 2628 CD Delft, The Netherlands (e-mail: R.Mirzadarani@tudelft.nl; Z.Li-20@tudelft.nl; Z.Qin-2@tudelft.nl; p.t.m.vaessen@tudelft.nl; p.bauer@tudelft.nl; M.Ghaffarianniasar@tudelft.nl).

Digital Object Identifier 10.1109/TIE.2025.3618838

1557-9948 © 2025 IEEE. All rights reserved, including rights for text and data mining, and training of artificial intelligence and similar technologies. Personal use is permitted, but republication/redistribution requires IEEE permission. See https://www.ieee.org/publications/rights/index.html for more information.

Authorized licensed use limited to: Eindhoven University of Technology. Downloaded on February 25,2026 at 15:24:01 UTC from IEEE Xplore. Restrictions apply.

This article has been accepted for inclusion in a future issue of this journal. Content is final as presented, with the exception of pagination.

TABLE I
METHOD EFFECTIVENESS AT MEDIUM-FREQUENCY FOR MV SST REMARKS

Method	Effectiveness at MF	Implementation Complexity	Tunability	Suitability for MV SSTs	Reported unbalancing reduction	Remarks
Parallel Disks (no Compensation) [1]	Low to Moderate	Low	Low	Moderate	-	Simple but leads to uneven current due to inductance differences. End-coil current and mid-coil current have >80% difference.
Geometrical Adjustments [7]	Low	High	Fixed	Low	13.6%	Not effective at MF due to constructional complexity.
Compensation Toroids (This Work)	High	Low to Moderate	High	High	98.44%	Easily tunable via magnets or auxiliary windings; validated experimentally.

detailed the benefits of using CTCs and parallel paths to manage high currents. However, there is a gap in the literature concerning the direct application of these techniques to medium-voltage, medium-frequency SSTs.

The present study introduces a novel method to mitigate imbalance current sharing issues by employing a number of series-connected compensation inductors for high-current windings such as parallel disks. The proposed method introduces a modular, scalable compensation scheme using toroidal cores, enabling disk-level current balancing without altering the transformer geometry. The approach further includes tunable inductance control via auxiliary windings, which allows real-time or design-phase optimization. These innovations offer a unique combination of frequency adaptability, practical integration, and experimental validation, distinguishing the method from existing techniques.

While additional inductance has been used for current balancing in prior work, this study introduces a modular, disk-level compensation method with tunable toroids decoupled from the core. The approach enables localized balancing without modifying the transformer geometry, making it practical for MV MFT applications. By addressing the high-current issues and proposing viable solutions, this research facilitates the development of more efficient and reliable SSTs for high-power applications, contributing to the broader goal of advancing sustainable energy technologies. The proposed method is compared with the existing approaches in Table I. Here, the current-imbalance ratio is defined as follows:

$$\Delta = \frac{\max_k |I_k| - \min_k |I_k|}{\text{mean}(|I_k|)} \tag{1}$$

where I_k is rms magnitude of the current in parallel element k (disk/coil) at the operating frequency. While prior studies have explored current balancing through geometric variations, transposed conductors, or winding arrangements, these approaches often face limitations in medium-frequency transformer applications due to increased losses, constructional complexity, and low tunability. Notably, existing compensation techniques do not address current unbalancing at the disk-level with precision or flexibility suitable for MV SSTs.

The rest of the present article is organized as follows: Section II discusses the issues associated with unbalanced current sharing in transformer windings. Section III presents the proposed method for mitigating unbalanced current sharing. Section IV provides details of the experimental verification, and Section V concludes the article.

II. UNBALANCING IN CURRENT SHARING

In a transformer feeding a high-current load, any current unbalancing between the phases or inside the winding between the parallel paths is not desired and must be mitigated as much as possible. Current unbalancing leads to extra losses and extra heat, especially at the hotspots of the transformer, raises the need for more complicated cooling systems, and generally, increases the total owning cost of the transformer. The unbalancing has more severe consequences in high-or medium-frequency transformers.

There are several methods to deal with the high current in the secondary side of a step-down transformer. In most cases, having several parallel paths for the current in the secondary is essential. These parallel paths can be along the conductor such as litz wires or CTCs with several strands and transposition to avoid extra losses. Alternatively, the parallel paths can be within the same disk in the winding. However, having more parallel paths, such as parallel disks for high-current applications, is essential. For all of the techniques, current balancing is vital since having poor current sharing results in extra loss and rising temperatures. This phenomenon is more severe in medium- or high-frequency transformers for two main reasons. Firstly, the higher the frequency, the higher the proximity and skin effect. Secondly, the unbalancing occurs because the difference in the inductances of parallel disks is more significant when the frequency is much higher than 50 Hz.

A. Unbalancing Due to Different Inductances

In the 2-D core of Fig. 1, the three parallel coils consist of only one turn each. The relative permeability of the core is significantly greater than 1 but still finite. The permeability of the core can be calculated as follows:

$$\mu_c = \mu_0.\mu_{rc} \tag{2}$$

where $\mu_0 = 4\pi \times 10^{-7}$ and μ_{rc} is the relative permeability of the core. The electrical conductivity of the coils is significantly greater than 1. The outer borders of the core are assumed to be magnetic insulations ($A_x = A_y = A_z = 0$). The inductance of each winding can be calculated as follows:

$$[V] = j\omega[L].[I] \tag{3}$$

Authorized licensed use limited to: Eindhoven University of Technology. Downloaded on February 25,2026 at 15:24:01 UTC from IEEE Xplore. Restrictions apply.

This article has been accepted for inclusion in a future issue of this journal. Content is final as presented, with the exception of pagination.

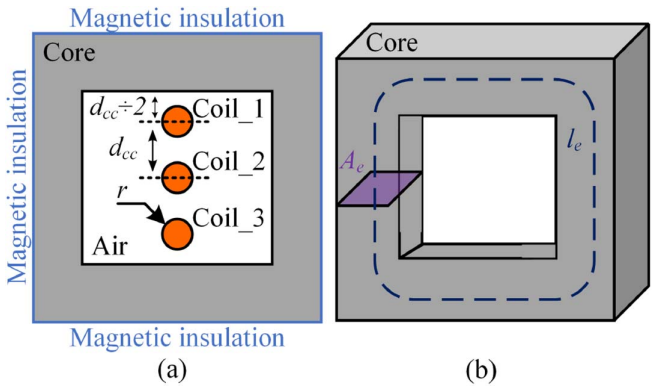

Fig. 1. (a) Simple 2-D problem with three parallel coils inside the core window; (b) 3-D view of a magnetic core illustrating the effective magnetic path length l_e and the effective cross-sectional area A_e.

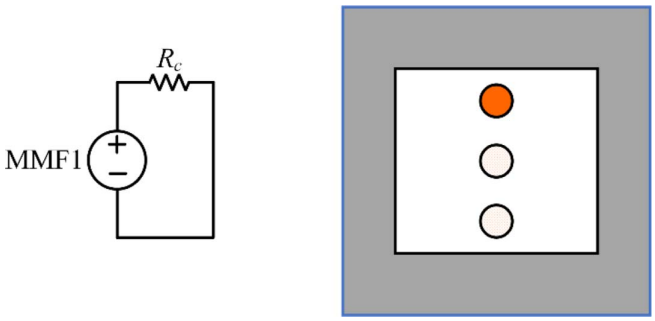

Fig. 2. Equivalent magnetic circuit when coil_1 is excited by a current and other coils are left open circuit ($I = 0$).

where ω is the angular frequency. $[V]$, $[L]$, and $[I]$ are the matrices of voltage, inductance, and current, respectively. For the three-coil problem, (3) can be written as follows:

$$\begin{bmatrix} V_1 \\ V_2 \\ V_3 \end{bmatrix} = j\omega \begin{bmatrix} L_{11} & L_{12} & L_{13} \\ L_{21} & L_{22} & L_{23} \\ L_{31} & L_{32} & L_{33} \end{bmatrix} . \begin{bmatrix} I_1 \\ I_2 \\ I_3 \end{bmatrix} . \tag{4}$$

The elements of the inductance matrix inductance $[L]$ consist of two parts as follows:

$$[L] = [L_c + L_a]. \tag{5}$$

According to (5), the inductances are made of two parts: one corresponding to the magnetic core (L_c) and one corresponding to the air (L_a). Since the relative permeability of the core is significant, it is obvious that $L_c >> L_a$.

L_c can be calculated using the equivalent magnetic circuit as shown in Fig. 2 as follows:

$$L_c = \frac{N^2}{R_c} = \frac{N^2 \mu_0 \mu_r A_e}{l_e} \tag{6}$$

where R_c is the equivalent reluctance of the core, A_e is the effective cross-section area of the core, and l_e is the effective length of the core as shown in Fig. 1(b).

While there are several studies investigating the inductance in the core window, such as [24], Calculating L_a is not straightforward. Moreover, both L_c and L_a can be calculated using finite elements method (FEM). In the present study, L_c and L_a are obtained using FEM simulation using COMSOL. The relationship between inductance and energy is as follows:

$$E = \frac{1}{2} L I^2 \tag{7}$$

where I is the current of the coil. L_c and L_a can be calculated as follows:

$$L_c = \frac{2}{I^2} \times \iiint_{\text{core}} W_{\text{mav}} . dv \tag{8}$$

$$L_a = \frac{2}{I^2} \times \iiint_{\text{window}} W_{\text{mav}} . dv \tag{9}$$

where W_{mav} is the time average of the magnetic energy density, and integrals are on the core and window for L_c and L_a, respectively. The L_c is the same, and the only difference is on L_a of them. Therefore, the inductance matrix has elements with values close to each other as follows:

$$L = \begin{bmatrix} L_c + L_{a11} & L_c + L_{a12} & L_c + L_{a13} \\ L_c + L_{a21} & L_c + L_{a22} & L_c + L_{a23} \\ L_c + L_{a31} & L_c + L_{a32} & L_c + L_{a33} \end{bmatrix} . \tag{10}$$

The condition number measures how much the output value of a function can change for a small change in the input. When the elements of a matrix like $[L]$ are close to each other, the matrix might have a high condition number, especially if the differences between the elements lead to the matrix being close to singular (i.e., its determinant is close to zero). This means that $[L]$ is ill-conditioned, and as a result, the inverse $[L]^{-1}$ can have elements with significant differences even if the elements of $[L]$ have small differences. At higher frequencies, the proximity effect increases the differences in effective inductance between parallel paths, which raises the condition number of the inductance matrix $[L]$ and amplifies the sensitivity of current distribution to small inductance variations. The proposed compensation method reduces this sensitivity by improving the conditioning of $[L]$.

In a winding with several parallel paths, the voltage of the parallel disks is forced to a fixed value since the ends of the windings are connected rigidly to the high-current busbars. If the voltages are assumed to be the same, currents can be calculated from (4) as follows:

$$[I] = \frac{1}{j\omega} . [V] \cdot [L]^{-1}. \tag{11}$$

Therefore, the currents can be varied significantly even though the inductances are almost equal. Analysis based on [24] and FEM proves that in winding around a magnetic core without an air gap consisting of several parallel coils (disks), the inductance of the upper and lower coils is lesser than the inductance of the inner coil. Therefore, the upper and lower coils will carry more current than the inner coils. This situation is depicted in Fig. 3.

B. The Impact of the Air Gap

The equivalent magnetic circuit, considering the air gap, will be changed which can modeled as an reluctances in series (r_g) [14], [24], [25]. The fringing effect, changes the field in

Authorized licensed use limited to: Eindhoven University of Technology. Downloaded on February 25,2026 at 15:24:01 UTC from IEEE Xplore. Restrictions apply.

This article has been accepted for inclusion in a future issue of this journal. Content is final as presented, with the exception of pagination.

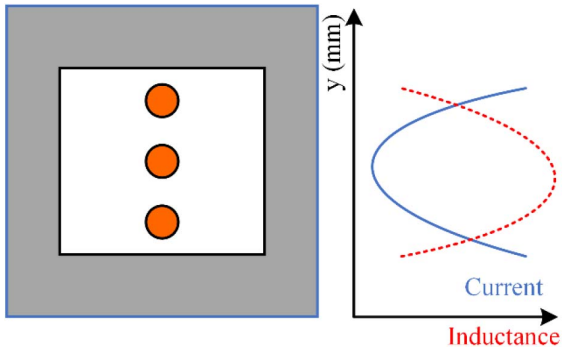

Fig. 3. Current sharing and inductance comparison of parallel coils (disks) of a winding around a nongapped magnetic core. The upper and lower coils have lesser inductance and higher current than the inner coil.

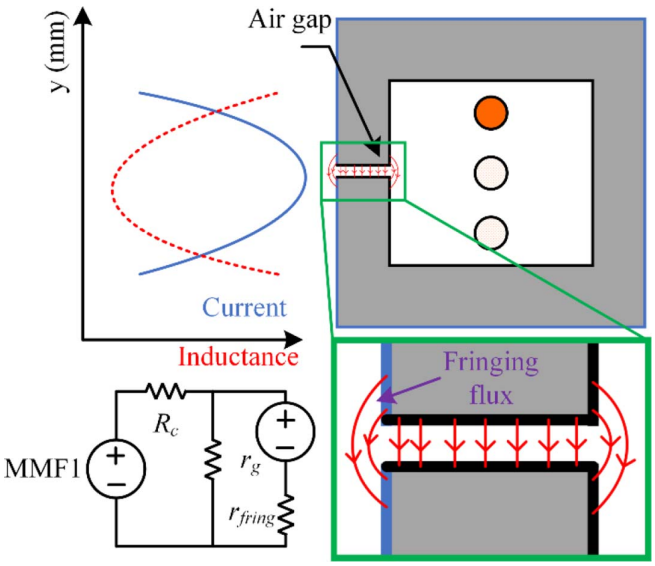

Fig. 4. Equivalent magnetic circuit of a gapped magnetic core considering the fringing effect. The upper and lower coils have higher inductance and lesser current than the inner coil.

the areas near the gap, can be modeled as a parallel branch consisting of a reluctance in series connection to an anti-MMF source in the equivalent magnetic circuit, as shown in Fig. 4. The coils nearer to the gap will be more affected by the fringing effect. This impact is shown in Fig. 5. The fringing effect leads to a nonuniform magnetic field distribution, causing variations in inductance across different coil positions. Coils closer to the gap experience reduced inductance due to the lower effective permeability in the fringing region, which increases the local magnetic reluctance. Since current follows the path of least impedance, lower inductance results in higher current flow in these coils. A theoretical justification for this can be found in magnetic circuit analysis and field distribution studies in gapped-core transformers [24], [25].

The impact of the air gap is illustrated in Fig. 6 using FEM-based COMSOL simulations. In Fig. 6(a), the core does not have any gap. Therefore, the flux uniformly flows the two legs (vertical parts) and two yokes (horizontal parts) of the core.

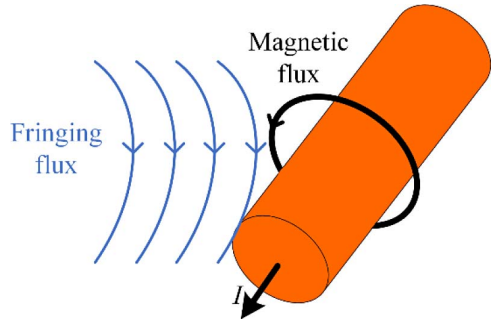

Fig. 5. Fringing effect near a current-carrying wire (the coil).

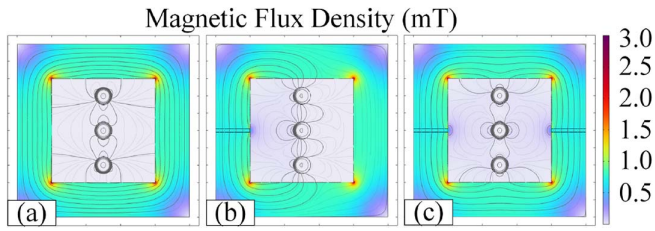

Fig. 6. FEM Simulation results of the impact of air gap in the core: (a) without gap; (b) air gap on one leg; and (c) air gaps on both legs.

In addition, the magnetic field inside the window is more intense near the upper and lower coils in comparison to the middle one. The higher the field intensity, the lesser the inductance and lesser the impedance, consequently. The lower impedance of two outermost coils leads to having higher current density through those coils. As soon as one of the legs of the core has an air gap, the situation differs form Fig. 6(a), which is depicted in Fig. 6(b). This also changes the magnetic field inside the window and has impact on the impedance of the coils. Nevertheless, for most of the real-world magnetic cores, both legs have air gaps as illustrated in Fig. 6(c), where the magnetic field intensity is higher near the middle coil which is located near the air gap. Again, the lesser the inductance the higher the current density in the coil.

III. Current Unbalancing Mitigation

Although there are other possibilities to achieve current balancing such as performing distributed air gaps through the magnetic core, the novel approach of the present study is to use series compensation inductors to achieve current balancing.

The impedance of a transformer winding is defined as follows:

$$Z = R_{\text{coil}} + j\omega L_{\text{coil}} \tag{12}$$

where $R_{\text{coil}} = R_{\text{coil_dc}} + R_{\text{coil_ac}}$, and L_{coil} is the inductance of the coil. For a transformer, the inductive part is dominant since the winding is designed to carry the current with minimum losses. At the measured operating point (1 kHz), the network is reactance-dominated ($|X|/R \approx 30$), and a normalized sensitivity analysis of $Z = R + \mathrm{j}\omega L$ shows that variations of the inductance matrix govern the branch currents: aggregated L-sensitivities

Authorized licensed use limited to: Eindhoven University of Technology. Downloaded on February 25,2026 at 15:24:01 UTC from IEEE Xplore. Restrictions apply.

This article has been accepted for inclusion in a future issue of this journal. Content is final as presented, with the exception of pagination.

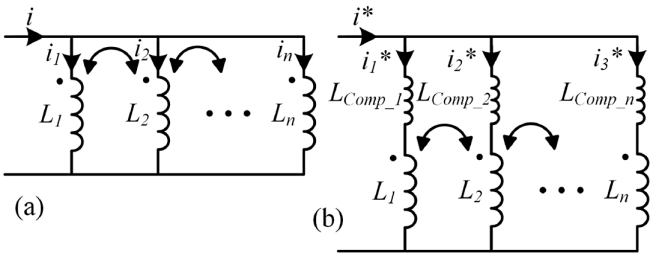

Fig. 7. Parallel coils as parallel connected coupled inductors: (a) without compensation; (b) with the compensation toroids.

are 80–124× larger than those of R (peaks ≈ 62–81 versus ≈ 0.66–1.20). Consistent ablation tests indicate that equalizing R reduces the relative current spread from 61% to 9.0%, whereas equalizing L reduces it to 0.52%, confirming that the observed imbalance at 1 kHz is primarily driven by L.

At 1 kHz, the added coils effect on both $[R]$ and $[L]$, however the inductance shifts dominate since max $\Delta L_{\text{diag}} = 5.34\ \mu$H versus max $\Delta R = 1.33\ \text{m}\Omega$, therefore $|\omega \Delta L|_{\max} \approx 33\ \text{m}\Omega$ is $\sim 25\times$ larger than $\Delta R_{\max}$. Accordingly, the compensation primarily modifies $[Z] = [R] + \text{j}\omega[L]$ through $[L]$, equalizing the effective reactances of the parallel paths and thereby reducing current unbalancing.

In the proposed winding, there are several coils (disks) parallel connected. All of the coils can be considered as coupled inductors since they are wounded around the same magnetic core. They are connected in parallel, therefore they can be considered as parallel connected aiding coupled inductors [Fig. 7(a)].

The currents can be derived from (11). Adding a compensation toroid to each coil adds extra inductance to it which does not share the same magnetic path with other coils and consequently, it is not coupled with them. Therefore, the inductance matrix can be rewritten as follows:

$$[L^*] = \begin{pmatrix} L_c + L_{a11} + L_{\text{comp_1}} & L_c + L_{a12} \cdots & L_c + L_{a1n} \\ \vdots & \ddots & \vdots \\ L_c + L_{an1} & L_c + L_{a2n} \cdots & L_c + L_{ann} + L_{\text{comp_n}} \end{pmatrix} \tag{13}$$

where L_{comp} is the inductance of the compensation toroid added to the coil. The new inductance matrix will determine the new currents as follows:

$$[I^*] = \frac{1}{j\omega} . [V] \cdot [L^*]^{-1}. \tag{14}$$

If the value of the compensation inductances selected suitable, the currents will be balanced. It is noteworthy that adding more than enough compensation inductance leads to "overcompensation" which can also increase unbalancing.

The idea of using toroids to compensate for the differences between the inductances of the parallel disks is depicted in Fig. 8. The method is described as follows. At the first turn of each coil, a toroidal magnetic core is placed to add the desired inductance to compensate for the differences between the inductances of parallel-connected coils. For the power transformers that do not have air gaps in the middle of the leg(s), the introduced compensation inductance will be higher for the top and bottom windings since these windings will carry more current without compensation. For the transformers made of cut cores similar to the prototype of the present study, the introduced inductance of the middle coil is selected higher since the middle coil is closer to the air gap of the core, has lesser inductance, and consequently carries more current.

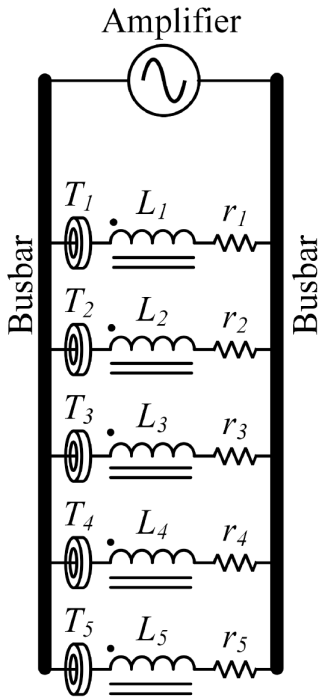

Fig. 8. Proposed method for mitigating current unbalancing in the parallel coils using compensation toroids.

The FEM simulation of the prototype is shown in Fig. 9. The inner coil carries more current since it has lesser inductance because of the presence of the gap in the magnetic core. Before applying the compensation toroids, the inner coil carried significantly more current in comparison to the other windings as shown in Fig. 9(b). However, after applying the compensation toroids, the current densities of the different coils become more similar to each other [Fig. 9(c)].

The value of the current that each coil carries before applying the proposed compensation inductors shows significant imbalance. These values are shown in Table II. Nevertheless, after applying the proposed compensation inductors, the value of the currents will be balanced significantly as shown in Fig. 9 and summarized in Table II.

The proposed method also has significant impact on the loss amount and distribution. The value of the loss before and after applying the proposed method can be calculated as follows:

$$\text{Loss}_{NC} = \sum_{n=1}^{N} R_n \times I_n^2 \tag{15}$$

$$\text{Loss}_{C} = \sum_{n=1}^{N} R_n^* \times I_n^{*2} \tag{16}$$

Authorized licensed use limited to: Eindhoven University of Technology. Downloaded on February 25,2026 at 15:24:01 UTC from IEEE Xplore. Restrictions apply.

This article has been accepted for inclusion in a future issue of this journal. Content is final as presented, with the exception of pagination.

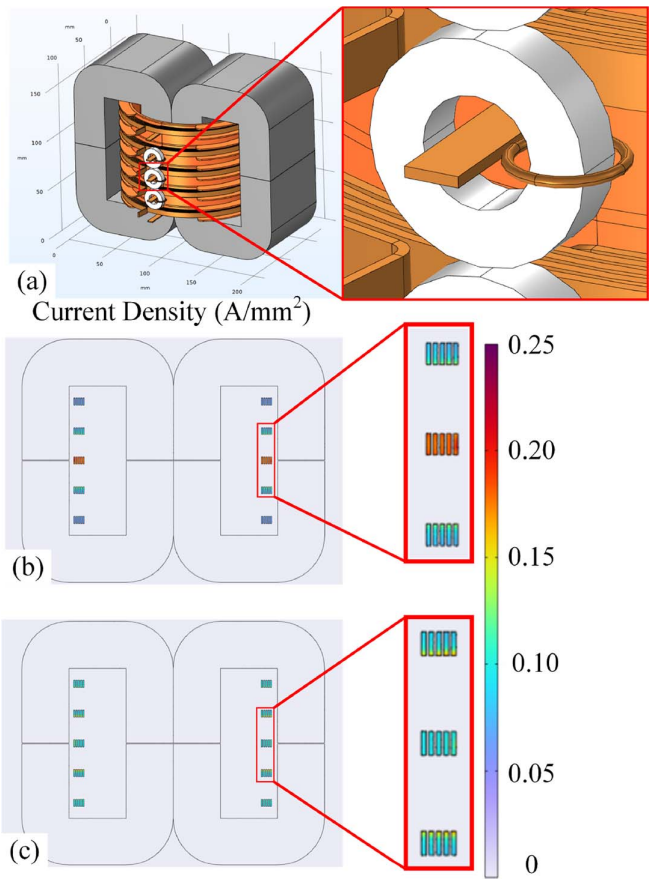

Fig. 9. FEM simulation for the prototype: (a) 3-D model and the compensation toroid; (b) current density (A/mm^2) over parallel-connected coils around the core before applying the compensation toroids; and (c) impact of applying compensation toroids.

TABLE II
SIMULATION RESULTS: THE VALUE OF THE ADDED COMPENSATION INDUCTANCES AND THE BALANCING SUMMARY AT 1 KHZ

Coil Number	Added Compensation Inductance (uH)	Equivalent Inductance (uH)	Current (mA_{rms})	
			Before	After
1	0	416.23	92.37	98.00
2	2.03	413.05	88.36	97.72
3	5.21	411.02	151.17	97.50
4	2.03	413.05	88.36	97.72
5	0	416.23	92.37	98.00

where N is the number of parallel coils, R_n is the ac resistance of the coil before compensation, and $R_n{}^*$ is the ac resistance of the coil after compensation. The losses are compared in Fig. 10 for the prototype at 1 kHz, illustrating that applying the compensation method decreases the loss by 28%. Nevertheless, it is not the only positive impact of the proposed method. For the compensated case the loss in the middle point, which is most likely the hotspot of the winding, is lesser, resulting in more balanced heat distribution and better overall thermal performance of the winding. Before compensation, the middle

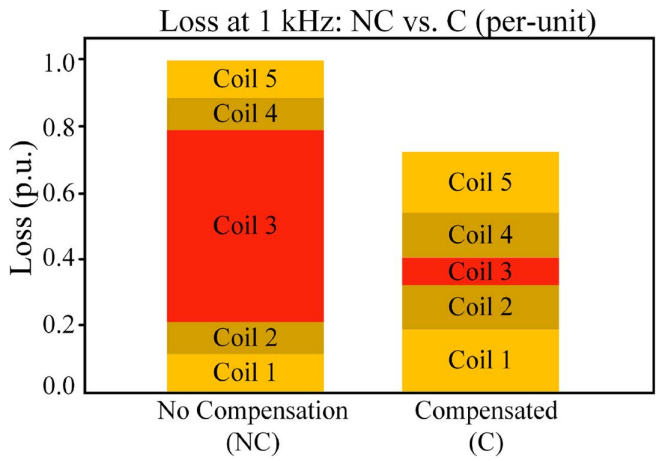

Fig. 10. Comparison of the losses of each coil before and after compensation.

disk carried ≈41% of $\sum I^2$;, but afterward each disk shares ≈20%, indicating uniform thermal loading. The small ferrite toroids add negligible loss and minimal coupling.

It is important to note that while the compensation toroids introduce additional inductance to each parallel winding, their values are carefully selected to be significantly smaller than the transformer's leakage inductance, typically in the range of 0.1% to 1%. This ensures that the added inductance has a negligible effect on the overall transformer behavior and does not interfere with the converter's performance in medium-frequency power conversion applications.

The compensation toroids are physically small and operate at relatively low flux densities. Given their limited core volume and use of low-loss ferrite material (e.g., 3E25), the additional core losses introduced are negligible in comparison to the winding and transformer core losses. Therefore, the method provides net improvement in efficiency by mitigating current unbalance and reducing associated localized losses.

The selection of the compensation toroid's parameters, such as core geometry, material, and number of turns, should be based on the required compensation inductance L_c, which in turn depends on the inductance mismatch ΔL between the parallel winding disks. A practical rule of thumb is to keep $L_{\text{comp}} << L_{\text{leakage}}$ (typically 0.1–1% of total transformer leakage inductance), to avoid interference with overall transformer behavior. The required L_{comp} can be calculated from

$$L_{\text{comp}} = L_{\text{ref}} - L_i \tag{17}$$

where L_{ref} is the highest inductance among all parallel paths and L_i is the inductance of the i-th disk. The value of the compensation inductance affects the current sharing; therefore, it is essential to fine-tune this value. For fine-tuning, an auxiliary winding is employed to control the inductance of the compensation toroid.

This method selected for the present study's experimental validation since it is excellent for controlling the current sharing of the winding, especially in overcoming hotspot temperature rise issues.

Authorized licensed use limited to: Eindhoven University of Technology. Downloaded on February 25,2026 at 15:24:01 UTC from IEEE Xplore. Restrictions apply.

This article has been accepted for inclusion in a future issue of this journal. Content is final as presented, with the exception of pagination.

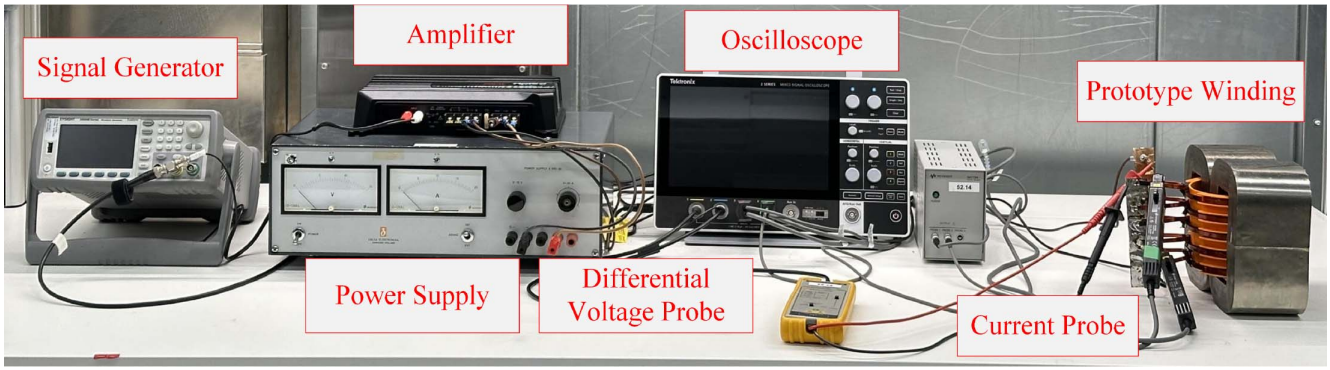

Fig. 11. Test table.

Each coil's inductance can be partitioned using FEM as follows:

$$L_i = L_{c,i} + L_{a,i} \tag{18}$$

where $L_{c,i}$ is the core-path term and $L_{a,i}$ arises from the window field. The observed mismatch ΔL is dominated by ΔL_a. The compensators add a diagonal matrix $[D] = \mathrm{diag}(L_{\mathrm{comp},i})$, yielding $[L]^* = [L] + [D]$, and $I \approx (\mathrm{j}\omega)^{-1}[L^*]^{-1}[V]$ for the tested frequencies. Because the disks are bus-bar forced to identical voltages, balancing is achieved when the row sums of $[L^*]^{-1}$ become equal. Selecting $L_{\mathrm{comp},i} = L_{a,j} - L_{a,i}$, equalizes the driving-point reactances and improves the conditioning of $[L]$, which reduces the sensitivity of $[I]$ to coil-to-coil differences. FEM-computed $L_{a,i}$ and experiments confirm that this choice suppresses current spread at 1 kHz, for instance, and remains effective, with appropriate tuning, across frequency changes.

IV. Experimental Validation

A. Prototype Winding

A prototype is made to prove the reasoning behind and analyze the unbalancing of the current sharing and mitigation methods. The winding is made of five parallel disks, each with five turns. The winding is made around a 3-D-printed polylactic acid (PLA) bobbin. The coils' turns are made of a 1 × 5 mm rectangular enameled conductor to ensure the fixed position of each turn in the disk. All disks are connected to high-current busbars for a solid and reliable parallel connection.

The magnetic core comprises two AMCC1000 amorphous cores (four pieces) with a shell-type core structure. The core is made of several layers of Metglas alloy, which provide a good lamination feature. However, the core is a cut-core, and there is a gap between the parts, affecting the current sharing of the parallel disks. The prototype is shown in Fig. 12.

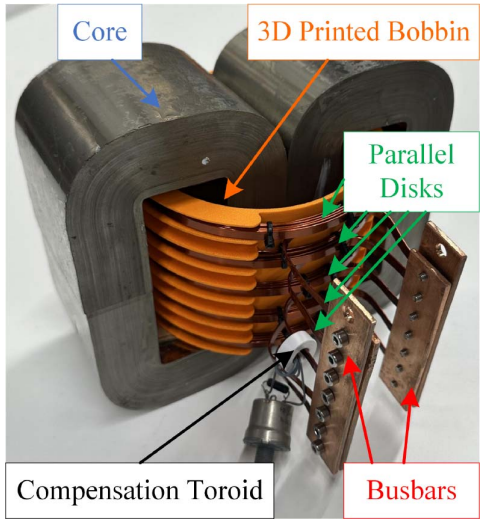

Fig. 12. Prototype.

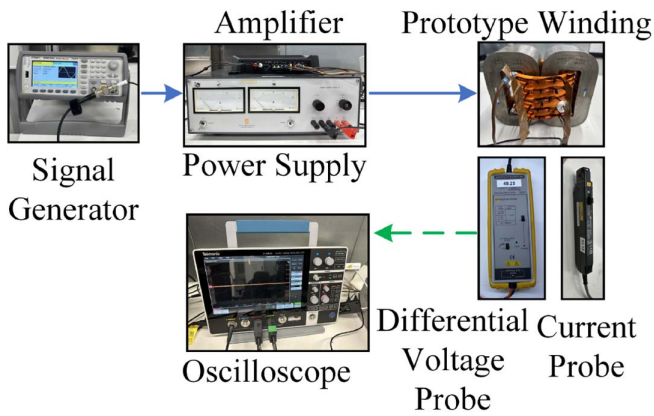

Fig. 13. Test setup block diagram.

B. Test Setup

The measuring setup consists of seven different parts as follows.

1) Signal generator (Keysight 33500B).
2) Power supply (Delta Elektronika 15 V, 20 A).
3) Amplifier (Sony Xplod 500 W).
4) Oscilloscope (Tektronix 2 Series MSO 4x 200 MHz 2.5GSPS).
5) Differential voltage probes (Picotech TA057).
6) Current probes (Keysight N2783B).
7) The prototype winding and core.

Authorized licensed use limited to: Eindhoven University of Technology. Downloaded on February 25,2026 at 15:24:01 UTC from IEEE Xplore. Restrictions apply.

This article has been accepted for inclusion in a future issue of this journal. Content is final as presented, with the exception of pagination.

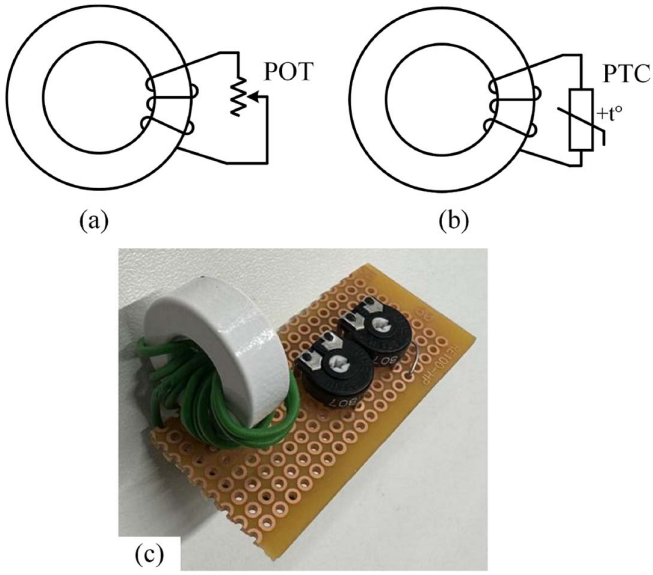

Fig. 14. Compensation toroids using auxiliary winding as fine-tuning method: (a) using a potentiometer; (b) using a positive-temperature-coefficient (PTC) thermistor; and (c) the prototype compensation toroid.

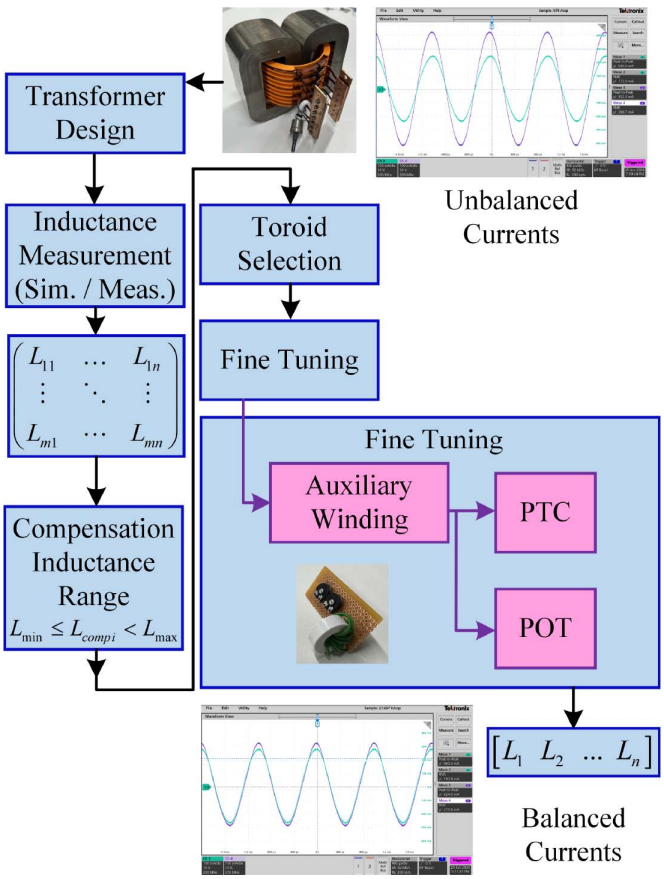

Fig. 15. Flowchart of presented method. The designed transformer might face unbalancing in current distribution. The compensation inductances are designed and fine-tuned to achieve current balancing.

The test table is shown in Fig. 11 and the block diagram of the test setup is shown in Fig. 13. The test is done under 1–10 kHz frequency.

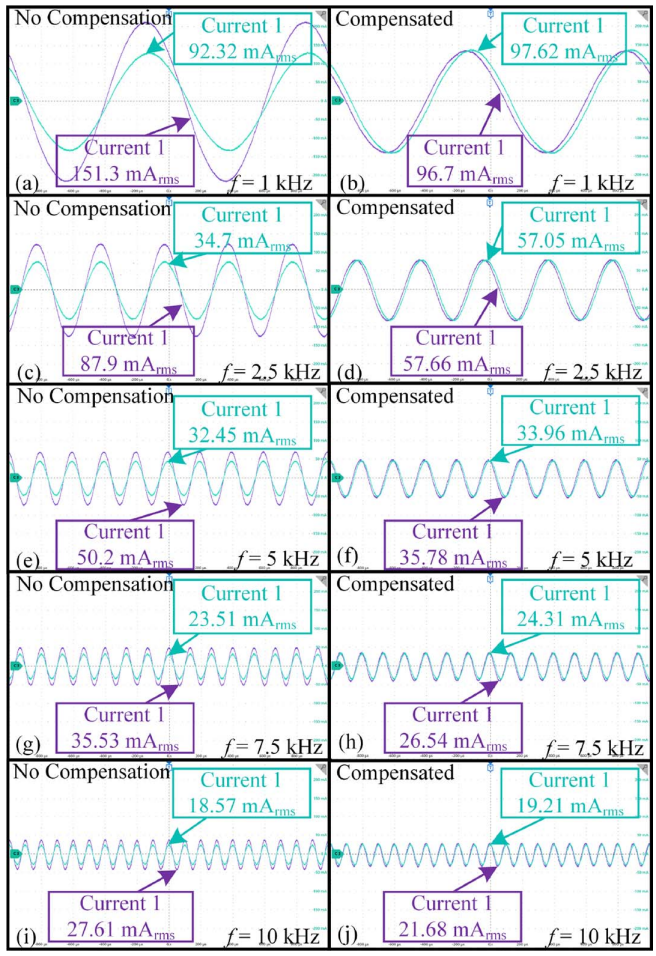

Fig. 16. Experimental results before and after applying compensation toroids at 1, 2.5, 5, 7.5, and 10 kHz.

C. Compensation Toroid Fabrication and Fine-Tuning

The compensation toroid using the auxiliary fine-tuning method is shown in Fig. 14. The compensating toroid must be designed considering the expected current carried by each coil. However, the variation in current between the parallel paths mainly originates from differences in their inductances.

The toroid core is a TN19/11/10 ferrite core, made of 3E25 material, with an AL value of 6420 nH/N^2. Ferrite was selected due to its low core losses and high resistivity, making it a suitable and efficient material for medium-frequency applications where eddy currents and magnetic losses must be minimized.

D. Experimental Results

The values of the inductances of the coils are as follows:

$$L_{\text{coils}} = [416.23 \ 413.05 \ 411.02 \ 413.05 \ 416.23] \ \mu\text{H}. \quad (19)$$

The value of the inductances of the coils should be as equal as possible to guarantee a good current-sharing. Therefore, the values of compensation inductances must be as follows:

$$L_{\text{comp}} = [0 \ 2.03 \ 5.21 \ 2.03 \ 0] \ \mu\text{H}. \quad (20)$$

Authorized licensed use limited to: Eindhoven University of Technology. Downloaded on February 25,2026 at 15:24:01 UTC from IEEE Xplore. Restrictions apply.

This article has been accepted for inclusion in a future issue of this journal. Content is final as presented, with the exception of pagination.

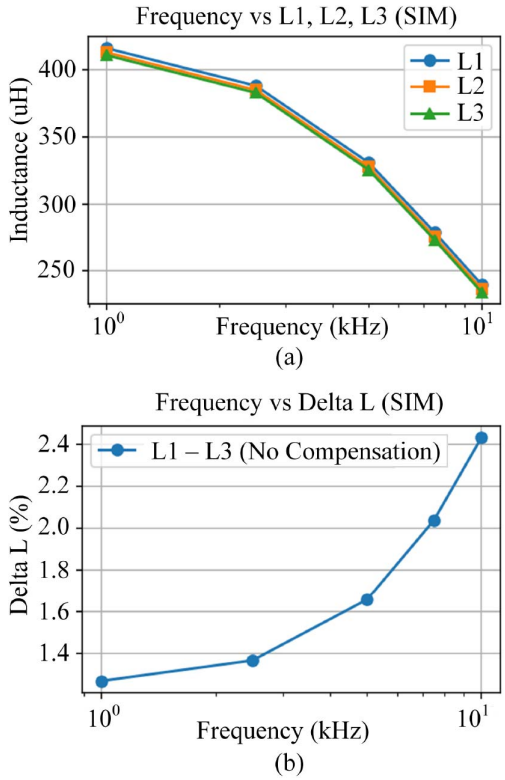

Fig. 17. (a) Changes of the inductances of the coils over frequency; and (b) difference in inductance between coil #1 and coil #3 at different frequencies without compensation. The mismatch increases at higher frequencies, emphasizing the need for frequency-specific compensation.

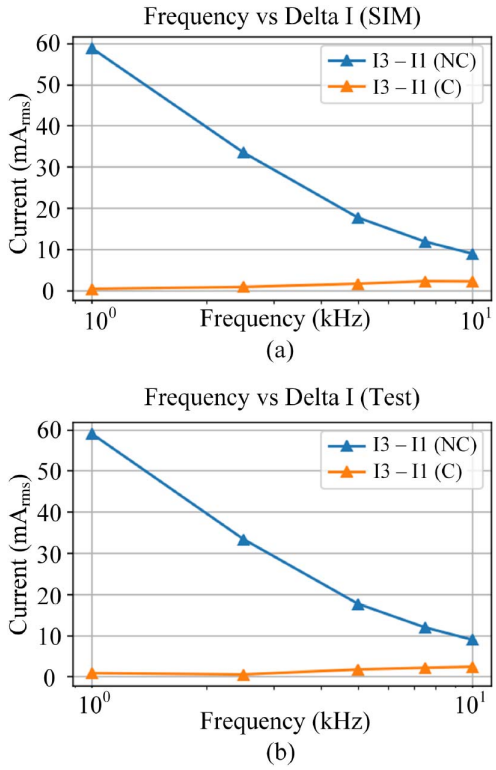

Fig. 18. Simulation versus experimental results: (a) difference between currents of coil #1 and coil #3 at various frequencies with (C) and without compensation (NC); and (b) the same results from experiments. The compensated case maintains minimal imbalance across frequencies, demonstrating the effectiveness of the tuning method.

The inductance of compensation toroid can be adjusted from 0.46 μH (auxiliary winding is short circuit) to 6.4 μH (auxiliary winding is open circuit). For coils #1 and #5 no compensation toroid is needed. For coils #2 and #4 the potentiometer of auxiliary winding is set to have 2.03 μH compensation inductance, and for coil #3, the compensation inductance is set to 5.21 μH. The flowchart of the presented method is shown in Fig. 15.

To assess the potential influence of stray magnetic coupling between the toroidal compensation inductors, FEM simulations are performed on the complete assembly. All coefficients are below 0.6%, confirming that mutual coupling between toroids is negligible. This validates the assumption that the toroidal inductors can be modeled as decoupled elements in both analysis and implementation.

The difference between the currents of upper disk (D_1) and the middle disk (D_3) before adding the compensation toroid is compared in Fig. 16. This figure compares the trend after adding the compensation toroid showcasing the balance in the current sharing between the disks #1 and #3.

Although the experimental validation in this work has been conducted at 1, 2.5, 5, 7.5, and 10 kHz, the proposed current balancing method is not limited to these frequencies. The selected frequency range is based on a system-level optimization for large-scale green hydrogen production using solid-state transformers (SSTs). In this application, high-current medium-frequency transformers (MFTs) are needed to supply large electrolyzers from medium-voltage offshore wind power. For operation beyond 10 kHz, particularly in the >100 kHz range, the proposed method remains conceptually valid, however design considerations such as increased ac resistance, reduced skin depth, and tighter layout constraints must be addressed when selecting and tuning the compensation toroids. When these factors are addressed, the compensation technique remains effective across a broad frequency range. Due to the high secondary current levels, the transformer design shares similarities with arc furnace transformers, requiring careful tradeoffs between frequency, size, and thermal management. Operation at higher frequencies leads to reduced transformer size but increases proximity and skin effects, which in turn require more complex cooling systems. Fig. 17 shows that while the absolute difference between winding inductances decreases with frequency, the percentage mismatch becomes more significant. This variation necessitates frequency-specific compensation.

As demonstrated in Fig. 18, the compensation elements can be tuned to maintain effective current sharing across the frequency range. These results confirm that the proposed compensation method remains effective under higher-frequency operation, provided that proper tuning is applied during the design phase.

Authorized licensed use limited to: Eindhoven University of Technology. Downloaded on February 25,2026 at 15:24:01 UTC from IEEE Xplore. Restrictions apply.

This article has been accepted for inclusion in a future issue of this journal. Content is final as presented, with the exception of pagination.

V. Conclusion

The proposed current balancing techniques demonstrate effective mitigation of current unbalancing in high-current windings of medium-frequency SSTs. By implementing compensation toroids, significant improvements in current sharing were observed, reducing the risks associated with hotspots and enhancing the overall efficiency of the transformer. The experimental validation confirms that these methods can be adapted to medium-frequency applications, providing a practical approach for optimizing transformer performance in high-power scenarios.

The improved current sharing demonstrated across all tested frequencies suggests a significant reduction in ac winding losses, particularly those associated with proximity and circulating currents. Future work will include direct efficiency and thermal characterizations to quantify the full impact on transformer performance. While the proposed method introduces minor additional components, a future study will evaluate the system-level tradeoffs between winding loss savings and any added material or core losses, including cost optimization strategies for scalable industrial applications.

References

[1] H. Wang, Q. Yang, Y. Li, J. Wang, D. Yuan, and M. Hu, "Electromagnetic characteristic calculation of several parallel coils for high current transformer based on field-circuit coupling method," *IEEE Trans. Appl. Supercond.*, vol. 29, no. 2, pp. 1–5, Mar. 2019, doi: 10.1109/TASC.2019.2893706.

[2] Z. Li et al., "Medium-voltage solid-state transformer design for large-scale H2 electrolyzers," *IEEE Open J. Power Electron.*, vol. 5, pp. 936–955, 2024, doi: 10.1109/OJPEL.2024.3414151.

[3] R. Mirzadarani et al., "Three-phase medium-voltage medium-frequency transformer for SST in green hydrogen production," *Presented at IECON 2023 - 49th Annu. Conf. IEEE Ind. Electron. Soc.*, Singapore, Singapore, 2023, pp. 1–6.

[4] R. Mirzadarani, Z. Li, Z. Qin, P. Vaessen, P. Bauer, and M. G. Niasar, "Symmetrical transformer for medium-voltage medium-frequency ISOP three-phase LLC SST," in *Proc. IEEE 10th Int. Power Electron. Motion Control Conf. (IPEMC2024)*, May 2024, pp. 3246–3251, doi: 10.1109/IPEMC-ECCEAsia60879.2024.10567857.

[5] Z. Li et al., "Comparison of modular multilevel converter based solid state transformer for ac/dc application," in *Proc. 49th Annu. Conf. IEEE Ind. Electron. Soc., (IECON)*, Oct. 2023, pp. 1–6, doi: 10.1109/IECON51785.2023.10312314.

[6] G. Haritha, K. Sundaramoorthy, and A. Sankar, "Xilinx system generator-based rapid prototyping of solid-state transformer for on-grid renewable energy integration," *IEEE J. Emerg. Sel. Topics Power Electron.*, vol. 9, no. 2, pp. 1280–1289, Apr. 2021, doi: 10.1109/jestpe.2019.2963277.

[7] V. Nabaei, S. A. Mousavi, K. Miralikhani, and H. Mohseni, "Balancing current distribution in parallel windings of furnace transformers using the genetic algorithm," *IEEE Trans. Magn.*, vol. 46, no. 2, pp. 626–629, Feb. 2010, doi: 10.1109/TMAG.2009.2031980.

[8] A. Anurag, S. Acharya, and S. Bhattacharya, "Solid state transformer for medium voltage grid applications enabled by 10 kV SiC MOSFET based three-phase converter systems," in *Proc. IEEE 12th Energy Convers. Congr. & Expo.-Asia (ECCE-Asia)*, Piscataway, NJ, USA: IEEE Press, 2021, pp. 906–913.

[9] H. S. Krishnamoorthy, P. N. Enjeti, and J. J. Sandoval, "Solid-state transformer for grid interface of high-power multipulse rectifiers," *IEEE Trans. Ind Appl.*, vol. 54, no. 5, pp. 5504–5511, Sep./Oct. 2018, doi: 10.1109/TIA.2017.2786257.

[10] B. Stojčić and D. Miljavec, "Current distribution in the low-voltage winding of the furnace transformer," *Int. J. Electr. Power Energy Syst.*, vol. 43, no. 1, pp. 1251–1258, Dec. 2012, doi: 10.1016/j.ijepes.2012.05.030.

[11] X. M. Lopez-Fernandez and L. A. Alvarez-Gomez, "Calculation of stray losses in continuously transposed conductor cable transformer windings by multi-slice methodology," *Int. J. Electr. Power Energy Syst.*, vol. 111, pp. 25–33, Oct. 2019, doi: 10.1016/j.ijepes.2019.03.038.

[12] B. Chen, X. Liang, and N. Wan, "Design methodology for inductor-integrated litz-wired high-power medium-frequency transformer with the nanocrystalline core material for isolated dc-link stage of solid-state transformer," *IEEE Trans. Power Electron.*, vol. 35, no. 11, pp. 11557–11573, Nov. 2020, doi: 10.1109/tpel.2020.2987944.

[13] K. S. Rama Rao and M. N. Karsiti, "Optimal design of a furnace transformer by intelligent evolutionary methods," *Electron. Power Energy Syst.*, vol. 43, pp. 1056–1062, Jul. 2012, doi: 10.1016/j.ijepes.2012.06.019.

[14] W. G. Hurley and W. H. Wölfle, *Transformers and Inductors for Power Electronics: Theory, Design and Applications*. Hoboken, NJ, USA: Wiley-Blackwell, 2013. [Online]. Available: http://site.ebrary.com/id/10660576

[15] J. Jiang, W. Chen, Y. Song, and Z. Shen, "Active control strategy of partial discharge for insulation of high-power high-voltage high-frequency transformers (H3Ts)," *IEEE Trans. Ind. Electron.*, vol. 70, no. 7, pp. 7521–7524, Jul. 2023, doi: 10.1109/TIE.2022.3203758.

[16] H. Abdoli, J. S. Moghani, S. Vaez-Zadeh, A. Babaki, A. J. Natanzi, and J. Rodríguez, "Multilevel inverter with a new modulation method applied to solid-state transformer in PV applications," in *Proc. 47th Annu. Conf. IEEE Ind. Electron. Soc. (IECON)*, Piscataway, NJ, USA: IEEE Press, 2021, pp. 1–6.

[17] A. Anurag, "HV SiC MOSFET enabled solid state transformers for mobile utility support equipment-based applications," North Carolina State Univ., 2021.

[18] A. Anurag, S. Acharya, Y. Prabowo, V. Jakka, and S. Bhattacharya, "Design of a medium voltage mobile utilities support equipment based solid state transformer (MUSE-SST) with 10 kV SiC MOSFETs for grid interconnection," in *Proc. 9th IEEE Int. Symp. Power Electron. Distrib. Gener. Syst. (PEDG)*, Jun. 2018, pp. 1–8, doi: 10.1109/PEDG.2018.8447766.

[19] H. Chen, A. Prasai, R. Moghe, K. Chintakrinda, and D. Divan, "A 50-kVA three-phase solid-state transformer based on the minimal topology: Dyna-C," *IEEE Trans. Power Electron.*, vol. 31, no. 12, pp. 8126–8137, Dec. 2016, doi: 10.1109/TPEL.2016.2518641.

[20] Q. Y. Huang et al., "500kVA hybrid solid state transformer (HSST): Architecture, functionality and control," in *Proc. 12th Annu. IEEE Energy Conversion Congress Exposit. (IEEE ECCE)*, Detroit, MI. Piscataway, NJ, USA: IEEE Press, 2020, pp. 4864–4871.

[21] Z. Li, E. Hsieh, Q. Li, and F. C. Lee, "High-frequency transformer design with medium-voltage insulation for resonant converter in solid-state transformer," *IEEE Trans. Power Electron.*, vol. 38, no. 8, pp. 9917–9932, Aug. 2023, doi: 10.1109/TPEL.2023.3279030.

[22] X. She, X. Yu, F. Wang, and A. Q. Huang, "Design and demonstration of a 3.6-kV-120-V/10-kVA solid-state transformer for smart grid application," *IEEE Trans. Power Electron.*, vol. 29, no. 8, pp. 3982–3996, Aug. 2014, doi: 10.1109/tpel.2013.2293471.

[23] X. Zhang, Y. Xu, Y. Long, S. Xu, and A. Siddique, "Hybrid-frequency cascaded full-bridge solid-state transformer," *IEEE Access*, vol. 7, pp. 22118–22132, 2019.

[24] T. Luo, M. G. Niasar, and P. Vaessen, "Two-dimensional frequency-dependent resistance and inductance calculation method for magnetic components with round conductors," *IEEE Trans. Magn.*, vol. 60, no. 1, pp. 1–11, Jan. 2024, doi: 10.1109/TMAG.2023.3340115.

[25] T. Luo, M. G. Niasar, and P. Vaessen, "2-D winding losses calculation for round conductor coil," *IEEE Trans. Power Electron.*, vol. 38, no. 4, pp. 5107–5117, Apr. 2023, doi: 10.1109/TPEL.2022.3230724.

Reza Mirzadarani (Student Member, IEEE) was born in Isfahan, Iran, in 1991. He received the M.Sc. degree in power systems from the University of Kashan, Kashan, Iran, in 2018. He is currently working toward the Ph.D. degree in electrical engineering with Delft University of Technology (TU Delft), Delft, The Netherlands.

He has worked on various high-voltage power electronics projects. His research interests include design of medium-voltage, medium-frequency transformers for solid-state transformers in green hydrogen production, partial discharge mitigation, and medium-frequency, medium-voltage testing techniques.

Mr. Mirzadarani was a winner of IEEE International Challenge in Design Methods for Power Electronics Excellent Innovation Award 2023.

Authorized licensed use limited to: Eindhoven University of Technology. Downloaded on February 25,2026 at 15:24:01 UTC from IEEE Xplore. Restrictions apply.

This article has been accepted for inclusion in a future issue of this journal. Content is final as presented, with the exception of pagination.

Zhengzhao Li (Student Member, IEEE) received the B.Sc. degree from Tongji University, Shanghai, China, in 2018, and the M.Sc. degree from Shanghai Jiao Tong University, Shanghai, China, in 2021, both in electrical engineering. He is currently working toward the Ph.D. degree in electrical engineering with Delft University of Technology, Delft, The Netherlands.

His research interests include design and modeling of solid-state transformers.

Zian Qin (Senior Member, IEEE) received the B.Sc. degree from Beihang University, Beijing, China, in 2009, the M.Sc. degree from Beijing Institute of Technology, Beijing, in 2012, and the Ph.D. degree from Aalborg University, Aalborg, Denmark, in 2015, all in electrical engineering.

In 2014, he was a Visiting Scientist with RWTH Aachen University, Aachen, Germany. He is currently an Associate Professor with the Department of Electrical Sustainable Energy, Delft University of Technology, Delft, The Netherlands. His research interests include power quality and stability of power electronics-based grids, solid-state transformers, and battery energy storage. He has authored more than 100 journal and conference papers, four book chapters, and several international patents, and has led or contributed to numerous European, Dutch national, and industrial projects. He has also delivered over ten invited tutorials and keynote talks at international conferences and industry events.

Dr. Qin serves as an Associate Editor of IEEE TRANSACTIONS ON POWER ELECTRONICS, IEEE TRANSACTIONS ON INDUSTRIAL ELECTRONICS, and IEEE JOURNAL OF EMERGING AND SELECTED TOPICS IN POWER ELECTRONICS. He is the Founding Chair of the IEEE Transportation Electrification Council Benelux Chapter and the Dutch National Member of the CIGRÉ WG 4.101 on Grid-Forming Energy Storage Applications. He has held leading roles in major conferences, including Technical Program Chair for IEEE-PEDG 2024, IEEE-PEDG 2023, IEEE-ISIE 2020, and IEEE-COMPEL 2020. His work has been recognized with the IEEE Open Journal of Power Electronics Prize Paper Award (2020–2023) and the IEEE International Challenge on Design Methods for Power Electronics Excellent Innovation Award (2023).

Peter Vaessen (Member, IEEE) received the M.Sc. degree (*cum laude*) in electrical power engineering from Eindhoven Technical University, Eindhoven, The Netherlands, in 1985.

In 1985, he joined KEMA (now a CESI brand). In his 40-year career, he held the research positions in the field of large power transformers and high-voltage measurement and testing. He headed the Transmission and Distribution High Voltage Department and managed realization projects, among them the construction of Dutch 400 kV substations and laboratory test facilities. As a Principal Consultant, he has 25 years of experience in (U)HVdc Technology and Transmission and Distribution Grids with high shares of renewables. He is the Manager of innovations with CESI and is actively involved in the technology strategy. He is the Chairman of the Board of the European Distributed Energy Resources Laboratories Association and a member of several national and international working groups. He is a part-time Professor of hybrid transmission systems with the Delft University of Technology, Delft, The Netherlands, where he teaches high-voltage technology and HVdc.

Pavol Bauer (Senior Member, IEEE) received the master's degree from the Technical University of Kosice, Kosice, Slovakia, in 1985, and the Ph.D. degree from Delft University of Technology, Delft, The Netherlands, in 1995, both in electrical engineering.

From 2002 to 2003, he was with KEMA (DNV GL), Arnhem, The Netherlands, on different projects related to power electronics applications in power systems. He is currently a Full Professor with the Department of Electrical Sustainable Energy, Delft University of Technology, and the Head of DC Systems, Energy Conversion, and Storage Group. He is also a Professor with Brno University of Technology, Brno, Czech Republic, and an Honorary Professor with the Politehnica University Timisoara, Timisoara, Romania. He has published over 180 journal articles and 450 conference papers in his field. He is an author or coauthor of eight books, holds seven international patents, and organized several tutorials at international conferences. He has worked on many projects for the industry concerning wind and wave energy, power electronic applications for power systems such as Smarttrafo; HVdc systems, projects for smart cities such as photovoltaic (PV) charging of electric vehicles, PV and storage integration, contactless charging; and he participated in several Leonardo da Vinci and H2020, and Electric Mobility Europe EU projects as a Project Partner (ELINA, INETELE, E-Pragmatic, Micact, Trolley 2.0, OSCD, P2P, and Progressus) and a Coordinator (PEMCWebLab.com-Edipe, SustEner, and Eranet DCMICRO).

Prof. Bauer is the Former Chairman of Benelux IEEE Joint Industry Applications Society, Power Electronics and Power Engineering Society Chapter, the Chairman of the Power Electronics and Motion Control Council, a member of the Executive Committee of European Power Electronics Association, and also a member of the International Steering Committee at numerous conferences.

Mohamad Ghaffarian Niasar (Member, IEEE) was born in Tehran, Iran, in 1984. He received the M.Sc. degree in electrical power engineering from Sharif University of Technology, Tehran, Iran, in 2008, and the Ph.D. degree in electrical engineering from the Royal Institute of Technology, Stockholm, Sweden, in 2015.

He is currently an Associate Professor with High Voltage Technologies Group, Delft University of Technology, Delft, The Netherlands. His research interests include the aging of electrical insulation, HVdc insulation system, partial discharges, high-frequency power transformers, power cables, and FEM modeling.

Authorized licensed use limited to: Eindhoven University of Technology. Downloaded on February 25,2026 at 15:24:01 UTC from IEEE Xplore. Restrictions apply.